K. M. Marks[1] and W. H. F. Smith[1]

[1]NOAA Laboratory for Satellite Altimetry, College Park, MD, USA.

Corresponding author: W. H. F. Smith (Walter.HF.Smith@noaa.gov)

Key Points:

- An automated method of stacking Sentinel-3 sea surface height data is documented
- Sentinel-3 A&B Pseudo-Low Rate Mode (PLRM) non-geoidal noise and stacked height noise is about 1.9 times that of Synthetic Aperture Radar Mode (SARM)
- Sentinel-3 A&B SARM and a PLRM median sea surface height profiles are available from the National Centers for Environmental Information data archive

Abstract

Sentinel-3 A&B radar altimeters yield sea surface height measurements in both a high-precision Synthetic Aperture Radar Mode (SARM), and a Pseudo-Low Resolution Mode (PLRM). We stacked repeat cycles from both missions and in both modes to compare their resolution of small seamounts. Stacking entailed removing non-geoidal heights and height errors, testing for consecutive measurements over ocean, aligning to common locations at 1 km intervals along a synthetic track, and forming a median height profile. These profiles are available from the National Centers for Environmental Information (NCEI) data repository. Global maps show that, over the oceans, the median height is usually derived from more than 49 cycles, and the typical error in an individual PLRM measurement is approximately 1.9 times greater than an individual SARM measurement. We applied a seamount detection bandpass filter to the median profiles and compared their spectral resolution to that of the Satellite for ARgos and AltiKa (SARAL) AltiKa mission. Small seamounts are similarly resolved by Sentinel-3 A&B SARM data and by the SARAL/AltiKa data.

1 Introduction

In this paper we stack sea surface height measurements from the ongoing radar altimeter missions Sentinel-3A (launched 16 February 2016) and Sentinel-3B (launched 25 April 2018), which are in sun-synchronous near-polar orbits that almost exactly repeat their measurement locations after every repeat cycle, one cycle being 385 orbits in 27 solar days. We form a synthetic ground track representing the typical measurement sequence path and align the data from each repeat cycle so as to assign each measurement to the synthetic track with minimal displacement. Each height value is then adjusted to remove large-scale departures from the geoid height caused by ocean dynamics and mis-modeled radar path delays. At intervals of 1 km along the synthetic track we then form the median, over all repeat cycles, of the adjusted heights. These median heights and related information are archived in, and available from, the National

Centers for Environmental Information (NCEI) (Marks & Smith, 2020a, 2020b, 2020c, 2020d).

In a previous study (Marks & Smith, 2018) we stacked sea surface height measurements from the Satellite for ARgos and AltiKa (SARAL) AltiKa radar altimeter mission, which differs from the Sentinel-3 A&B missions in the locations measured, the measurement posting rate, the number of repeat cycles available for stacking, and several features of the radar measurement system employed (Table 1).

Table 1. Key differences between the SARAL AltiKa and Sentinel-3 A&B altimeter missions

Characteristic	SARAL AltiKa	Sentinel-3 A&B
Radar Band (Carrier Frequency, GHz)	Ka (37)	Ku (13.6)
Measurement Mode(s)	LRM	PLRM & SARM
Measurement Posting Rate (Hz)	36.9 – 39.4	19.63
Orbit Repeat Cycle Interval (days)	35	27
Passes Per Repeat Cycle	1002	770
Number of Repeat Cycles Available	32	On-going

This paper describes aspects of our stacking method that are particular to the Sentinel-3 missions, as the aspects that are common with AltiKa are detailed in the previous paper. These radars measure sea surface height differently than conventional altimeters, and may improve the resolution of small geoid anomalies produced by small seamounts. The seamount resolution capability of AltiKa was compared to that of a conventional altimeter previously (Smith, 2015). Here, we compare the seamount anomaly resolution capabilities of the Sentinel-3 data to that of AltiKa.

2 Data

The altimeter data are from the Level-2 Non-Time Critical (NTC) Baseline Collection 004 (Sentinel-3 Team, 2013), and are of the water surface type generated by the European Organization for the Exploitation of Meteorological Satellites (EUMETSAT) Marine Centre (formerly named the Global Monitoring for Environment and Security (GMES) marine service) (Donlon, 2012). We extracted longitude, latitude, sea surface height, and time data from the NTC product, and used the Radar Altimeter Database System (RADS) (https://www.star.nesdis.noaa.gov/socd/lsa/RADS.php) to interpolate the surface classification flag and Earth Gravitational Model EGM2008 geoid values (Pavlis et al., 2012) to the data point longitude and latitude locations. The posting rate of the data is once per radar cycle, approximately 19.63 Hz; the sub-satellite point sweeps over the Earth's surface at about 6.68 km/s, so the nominal spacing between consecutive measurements is about 340 m along the sub-satellite ground track.

The radar altimeters on Sentinel-3 A&B have two operating modes, but can operate in only one or the other, exclusively, at any time. One, called the low resolution mode (LRM), functions as a conventional altimeter: radar pulses are emitted continuously at a pulse repetition frequency (PRF) of roughly 2 kHz, the power in received pulse echoes is averaged over each radar cycle (about 51 ms), and measurements are made from these power averages. The other, called the synthetic aperture radar (SAR) mode, emits pulses discontinuously, in "bursts:" each burst consists of 64 pulses emitted at a PRF of 17.825 kHz, but bursts are emitted at a rate of four per radar cycle, or approximately 78.5 Hz. Synthetic aperture processing of these echoes can narrow the measurement area on the sea surface and increase the measurement precision, and, depending on the extent of aperture synthesis employed, can synthesize either an unfocused "delay/Doppler" altimeter (Raney, 1998) or a fully-focused SAR altimeter (Egido & Smith, 2017).

For a time after Sentinel-3A was launched it collected some data in each mode, to calibrate and validate each. Sentinel-3B initially measured along the same ground track as Sentinel-3A, for purposes of inter-calibration of the two satellites; it later moved onto a new ground track interleaved with the Sentinel-3A track. We are interested in evaluating the SAR mode, and producing stacked data on both the original and interleaved tracks. We therefore have stacked Sentinel-3A data from repeat cycles 3 through 56, and Sentinel-3B data from repeat cycles 19 through 38, inclusive, as of this writing.

The data products we stacked provide two measurements of sea surface height, called SARM and PLRM. The SARM (for SAR mode) measurement uses unfocused delay/Doppler processing of the radar echoes. The same radar pulse echoes are also processed with the conventional algorithm to obtain a pseudo-LRM (PLRM) measurement; it is "pseudo" because a classical LRM altimeter pulses continuously and so makes more statistically independent measurements per radar cycle than does the discontinuous SAR mode. We stacked the height data in both the PLRM and SARM versions, in order to compare them, and in each case, we used the data at the full sampling rate given in the data products, approximately 19.625 Hz, and often called the "high rate" or "20-Hz" data.

Here, for comparison with our Sentinel-3 A&B stacks, we also show some data from our previous study stacking SARAL AltiKa data. Details on the data used and the stacking method are in Marks and Smith (2016; 2018). The AltiKa instrument pulses continuously and uses simple averages of power over radar cycles, as in a conventional (LRM-type) altimeter. However, where conventional altimeters employ a carrier frequency in the Ku radar band, AltiKa uses the higher frequency Ka radar band. This allows statistically independent measurements at a higher rate, and consequently the AltiKa PRF is about 3.66 kHz and independent measurements are posted at about 38.125 Hz (exact rates vary slightly as orbital altitude changes around the orbit). Additional features of the Ka measurement system also enhance the measurement precision (Smith, 2015).

3 Method

3.1 Synthetic ground track

We approximated the actual orbital motions of the Sentinel-3 A&B spacecraft with an idealized and simplified model in which the nodal period is exactly 1/385 of 27 mean solar days, the perigee remains frozen at the northernmost point in all orbits, and all departures from Keplerian elliptic motion are periodic within one orbital revolution (the only perturbations are "short period" in the sense of Kaula (1966)). With this simplification, each orbital revolution of the model motion sweeps out the same sequence of latitudes, and, relative to the equator crossing longitudes, each revolution sweeps the same sequence of relative longitudes. This allowed us to generate one "ascending" (northbound) and one "descending" (southbound) synthetic ground track "pass" (half revolution), and then to re-use these for each of the 770 passes in a repeat cycle by simply shifting the longitudes appropriately.

The sea surface height data products from the EUMETSAT Marine Center do not provide the satellite's positions over land. We therefore fit our simple motion model to the European Space Agency's reference orbits for the Sentinel-3A ground track and the interleaved track for Sentinel-3B, as these cover a complete repeat cycle with no sampling gaps. After model fitting, the synthetic ascending and descending passes were sampled at intervals of about 1 km along the ground track, such that each pass has 20,239 sample points between +/- 81.419 degrees latitude.

In our simple motion model, the ascending Equator crossing of each successive orbit lies 1/385 of 27 rotations westward of the one that preceded it, and likewise for each descending Equator crossing. We used this fact to determine all synthetic ground track Equator crossings by a best fit to the Equator crossings over ocean that were available in the data we stacked. Our simple motion model includes the effects of orbital eccentricity and so the time in flight over the northern hemisphere is less than half the nodal period; consequently, the descending equator crossings do not exactly bisect the ascending equator crossings, and therefore we fit the synthetic descending crossings separately from our fit of ascending crossings.

3.2 Data selection, alignment, and stacking

To facilitate band-pass filtering for seamount anomaly detection, our previous work stacking SARAL AltiKa (Marks & Smith, 2018) grouped data into chunks consisting of 1024 consecutive along-track points without gaps, an along-track distance of about 177.6 km. The Sentinel-3 data have a sampling rate roughly half that of AltiKa, and in the present study we set the data chunk length to 512 points, which is about 174 km along-track. Numbering these points from 1 to 512, the position of the 256th point is used in aligning selected data to a common point on the synthetic track for stacking and output.

Data alignment, adjustment to remove long-wavelength non-geoidal signals and errors, and stacking then proceed essentially as in our AltiKa study, except for the change of chunk length from 1024 to 512 points, and some changes in

the coding of the algorithm that sped up the computations without materially affecting the outcomes. The following is a recap; details are in Marks and Smith (2018; see particularly Figure 1 of that paper).

For all 770 passes of both Sentinel-3 A&B, and for every output point along the synthetic track, we look over all repeat cycles of input data available and for each repeat cycle we find the input measurement point closest to the synthetic output point. If this point is within ~1 km of the output point and if the 512 consecutive point chunk with this point as number 256 is complete without gaps and with all data flagged as valid ocean heights, then this chunk is selected. Note that, since consecutive data without gaps are spaced about 340 m apart, the alignment will not move the data more than ±170 m along-track. Proceeding in this way, for each output point we can assemble a matrix of data consisting of N column vectors, each column vector being 512 consecutive sea surface height points measured during one repeat cycle, and N will be the number of repeat cycles having data passing the alignment, contiguity, and validity criteria.

Where the output point is too close to land, or in areas of permanent sea ice cover, N will be zero; where N is not zero stacking continues as follows. For each column vector independently we form the differences in height between the observed heights in the column vector and the EGM2008 (Pavlis et al., 2012) geoid model heights at the corresponding latitudes and longitudes, we fit, robustly to outliers, a degree-two polynomial to the height differences, and we subtract the polynomial values from the values in the column vector. Note that this removes long-wavelength departures from the geoid, but does not remove the long-wavelength geoid itself; the heights removed may be due to ocean dynamics, mis-modeled or unaccounted for tides, barometric forcings, radar path delays, etc.

After adjusting all column vectors, taking the median across each row of the 512 by N matrix gives a 512-point column vector of median heights, the 256th element of which is the stacked output height. Subtracting the median height vector from each column vector in the 512 by N adjusted height matrix, taking absolute values of all elements, then taking the median of all absolute values in row 256, and scaling by 1.4826, gives an estimate of sigma ( ), the typical measurement error in a single measurement. Scaling by 1.4826 converts the median absolute deviation of a Gaussian distribution into that distribution's standard deviation; see Marks and Smith (2018).

Four NetCDF files containing the results of stacking the Sentinel-3 A&B SARM and PLRM data are archived at, and available for download from, the NCEI data repository (Marks & Smith, 2020a, 2020b, 2020c, 2020d). Each file contains 770 passes, each of which consists of 20239 records of longitude, latitude, N, , and stacked sea surface height.

3.3 Filtering

In our previous work (Marks & Smith, 2016, 2018) we attempted to identify small seamounts in stacked AltiKa repeat cycle data. This required application

of a Gaussian band-pass filter designed to pass seamount anomalies (~10 – 28 km full wavelength) to the sea surface height profiles. Here, we seek to compare the spectral resolution of seamounts in stacked repeat cycles from Sentinel-3 to those from AltiKa.

The procedure for filtering Sentinel-3 data entailed subtracting the slope from each 512-point stacked sea surface height profile to bring the endpoints to zero, and tapering with a Hamming window to minimize edge effects and spectral leakage in subsequent filtering operations. Then the Gaussian band-pass filter was applied via Fast Fourier Transform. The center point of the filtered profile (at location 256) is assigned to the appropriate synthetic track point.

We present products of our Sentinel-3 stacking project in the global maps section below, followed by sections that compare stacked height noise and spectral resolution with AltiKa stacking results.

4 Global Maps

Figures 1 - 4 show global maps of N and for Sentinel-3 A&B SARM and PLRM stacked data. These maps were created using GMT routine "blockmedian" (Wessel & Smith, 1998) to calculate the median number of cycles (and sigma values) in 1° x 1° grid cells, plotted on an Eckert IV projection.

Sentinel-3A maps of cycles in a stack (Figures 1a and 2a) show that, except for the polar regions where the number of cycles decreases due to rejections for sea ice and severe weather events, the majority of oceans are covered by stacks having 49 or more cycles. The slight reduction in cycles in equatorial regions (for example, light orange color grid cells in the western Pacific Ocean) reflect cycle rejections due to rain and tropical weather events. A number of grid cells along the Greenwich meridian (0° longitude) in both Sentinel-3A SARM (Figure 1a) and PLRM (Figure 2a) maps are blue colored, indicating they have a low number of cycles stacked. This is due to an open loop tracking command problem that occurred in Sentinel-3A cycles 1-26.

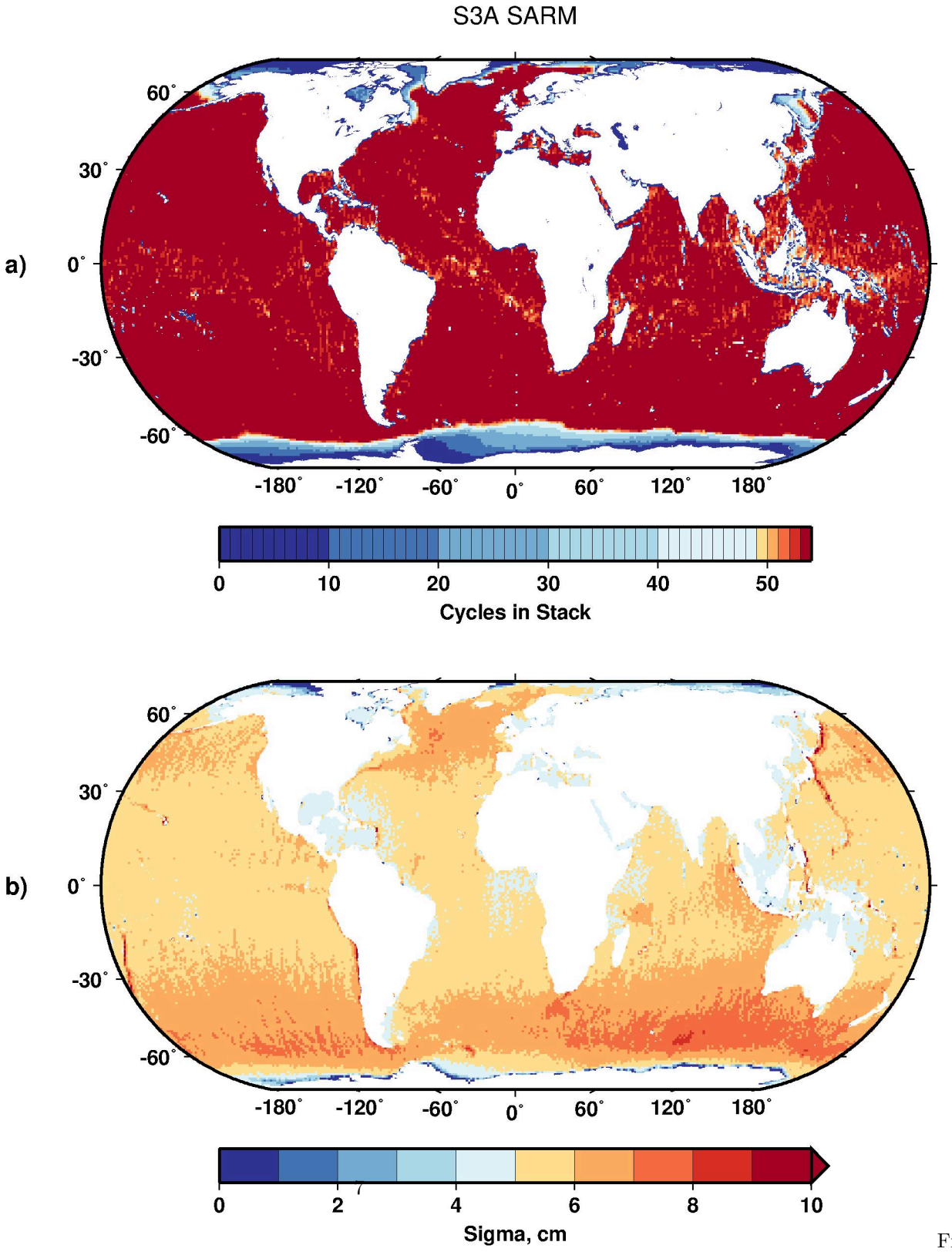
S3A SARM
a)
60˚
30˚
0˚
-30˚
-60˚
-180˚
-120˚
-60˚
0˚
60˚
120˚
180˚
0
10
20
30
40
50
Cycles in Stack
b)
60˚
30˚
0˚
-30˚
-60˚
-180˚
-120˚
-60˚
0˚
60˚
120˚
180˚
0
2
4
6
8
10
Sigma, cm

Figure

1. Global maps of Sentinel-3A SARM (a) number of cycles stacked and (b) sigma, the expected error in a single measurement.

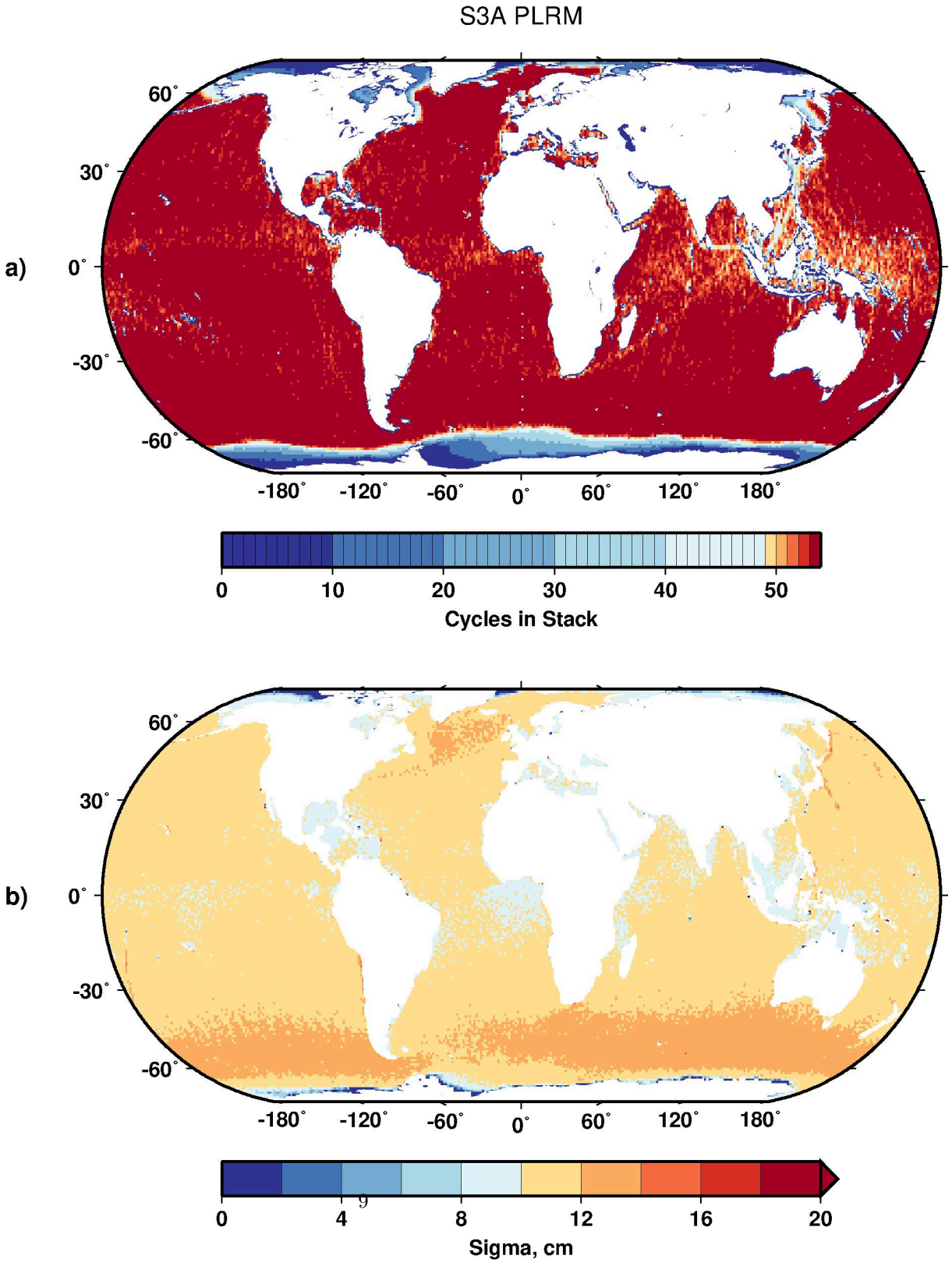
S3A PLRM
a)
60˚
30˚
0˚
-30˚
-60˚
-180˚
-120˚
-60˚
0˚
60˚
120˚
180˚
0
10
20
30
40
50
Cycles in Stack
b)
60˚
30˚
0˚
-30˚
-60˚
-180˚
-120˚
-60˚
0˚
60˚
120˚
180˚
0
4
8
12
16
20
Sigma, cm

Figure 2. Same as Figure 1 caption but for Sentinel-3A PLRM.

Sentinel-3B maps (Figures 3a and 4a) similarly show a decrease in number of cycles stacked in the polar regions, but with most ocean areas covered by stacks with 18 or more cycles. Along the equatorial latitudes is the slight reduction in cycles that reflects rejections due to rain and tropical weather events. The regular pole-to-pole track-like pattern of cells having 19 or 20 cycles in a stack is due to cycle 19 being incomplete.

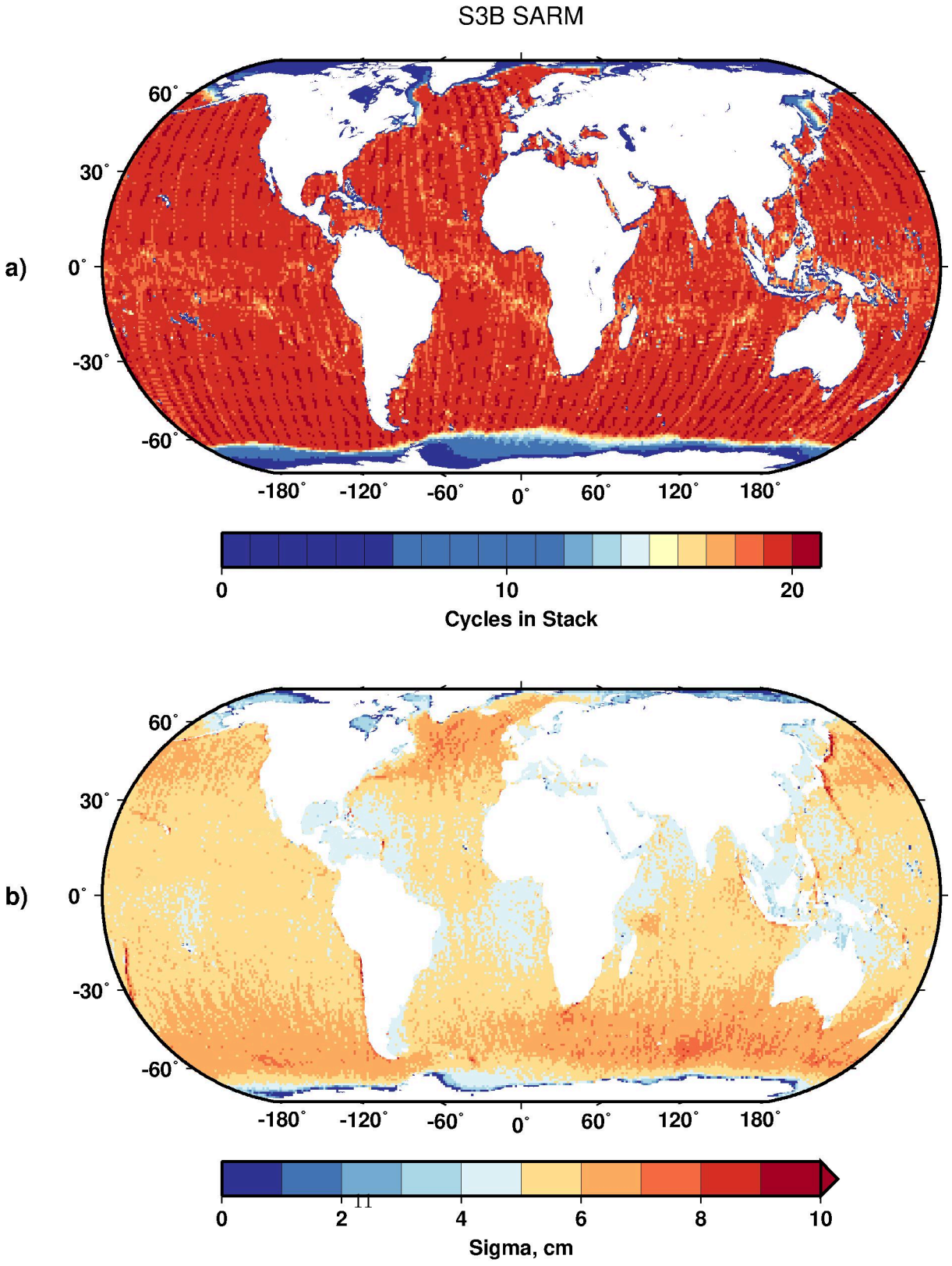
S3B SARM
a)
60˚
30˚
0˚
-30˚
-60˚
-180˚
-120˚
-60˚
0˚
60˚
120˚
180˚
0
10
20
Cycles in Stack
b)
60˚
30˚
0˚
-30˚
-60˚
-180˚
-120˚
-60˚
0˚
60˚
120˚
180˚
0
2
4
6
8
10
Sigma, cm

Figure 3. Same as Figure 1 caption but for Sentinel-3B SARM.

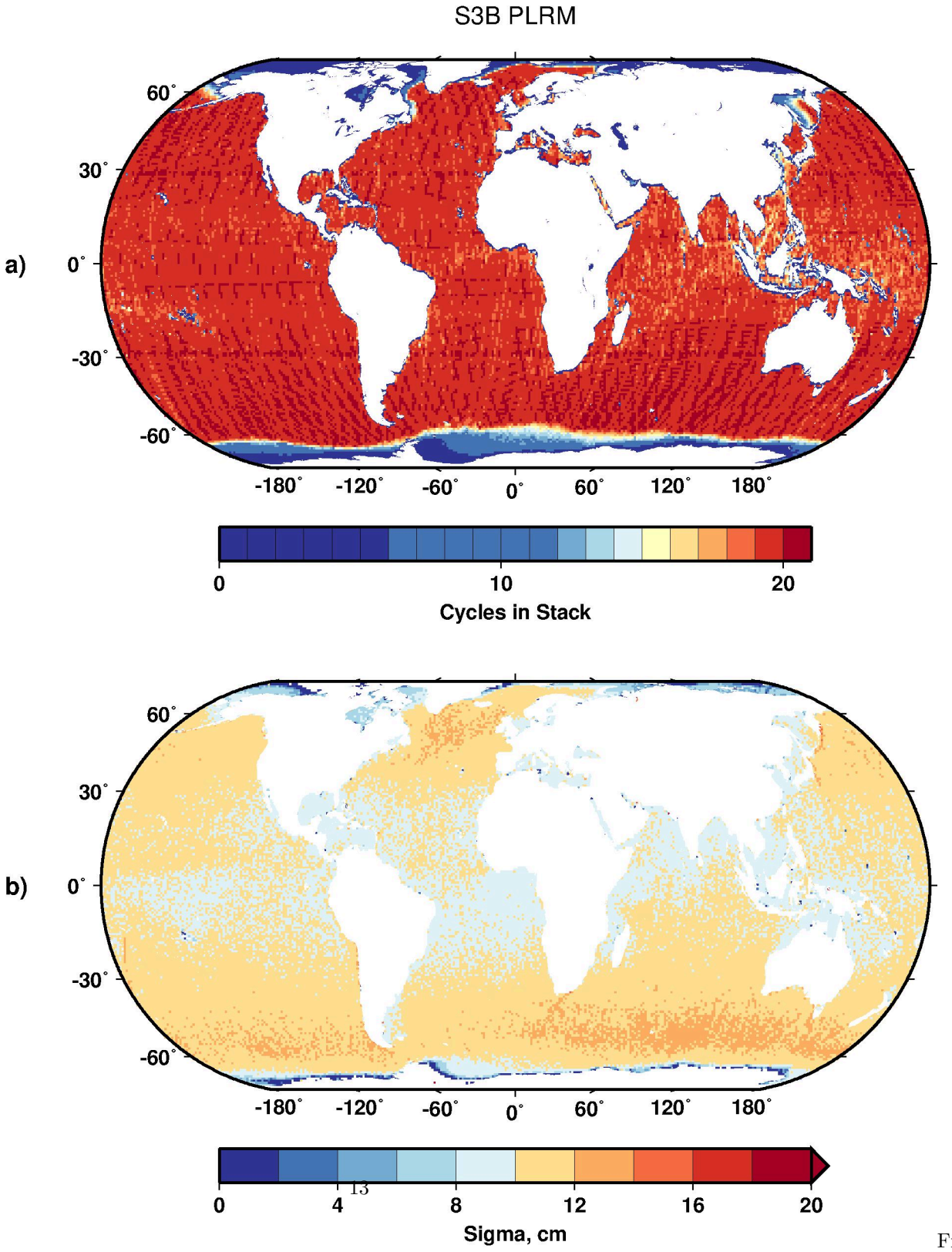
S3B PLRM
a)
60˚
30˚
0˚
-30˚
-60˚
-180˚
-120˚
-60˚
0˚
60˚
120˚
180˚
0
10
20
Cycles in Stack
b)
60˚
30˚
0˚
-30˚
-60˚
-180˚
-120˚
-60˚
0˚
60˚
120˚
180˚
0
4
8
12
16
20
Sigma, cm

Figure

4. Same as Figure 1 caption but for Sentinel-3B PRLM.

Global maps of , the expected error in a single measurement, are shown for Sentinel-3A in Figures 1b and 2b, and for Sentinel-3B in Figures 3b and 4b. The values generally increase with latitude, probably due to increasing roughness of the median sea state. For both Sentinel-3 A&B, the sigma values for PLRM are approximately 1.9 times that of SARM.

Figure 5 shows stacked sea surface heights (SSH) for Sentinel-3A SARM. The global anomaly pattern matches published geoid anomaly maps (e.g., Pavlis et al., 2012) because stacked sea surface height profiles that have had long-wavelength non-geoidal signal removed are essentially geoid height profiles.

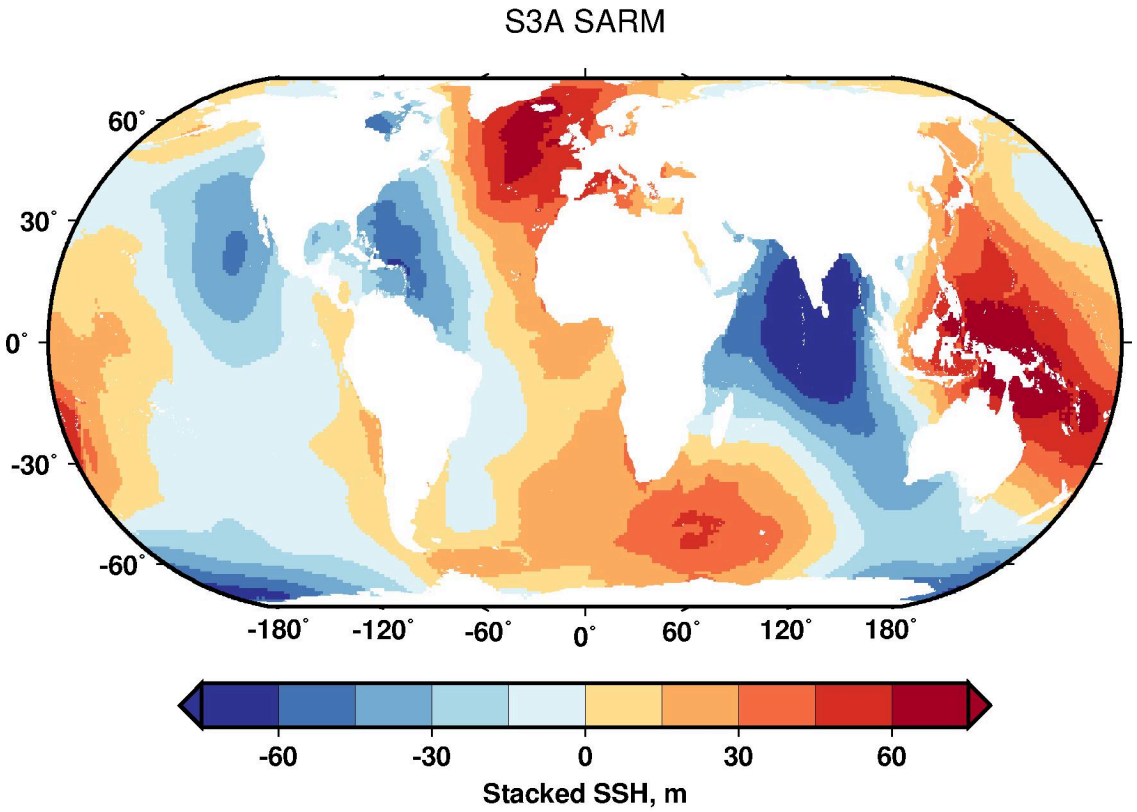

Figure 5. Global map of Sentinel-3A SARM stacked sea surface height, which is representative of comparable -3A PLRM, -3B SARM, and -3B PLRM maps.

5 Stacked Height Noise

For any number of cycles stacked, N, from 1 to half the total number of cycles used in our study, we can randomly assign individual cycles to either one of two groups, run the procedure in Section 3.2 on each group separately, and thus obtain two height profiles from "half-stacks" of N cycles each; repeating this

multiple times with independent random assignments each time then generates a "Monte Carlo" experiment yielding multiple realizations of pairs of stacked profiles. We did this and ensemble-averaged the intra-pair statistics across all realizations as a way of estimating the noise of a stacked height profile generated from a stack of N cycles. We call this noise estimate the "stacked height noise" and label it $_{\mathbf{N}}$, to distinguish it from the sigma defined above, which characterizes the uncertainty in height in a single repeat cycle after the column vector adjustment process described in Section 3.2. One expects that $_{\mathbf{N}}$ decreases as N increases.

The expected relationship has the form $_{\mathbf{N}} = \mathbf{B}\left[\frac{(\mathbf{2N+1})}{\mathbf{3}}\right]^{\frac{-\mathbf{1}}{\mathbf{2}}}$ rather than $_{\mathbf{N}} \propto \mathbf{N}^{\frac{-\mathbf{1}}{\mathbf{2}}}$ because the stacking and noise estimating processes are using medians rather than means. The expected value for $\mathbf{B}$ is , and fitting a curve of this form (Figure 6) to estimate B gives another (more overall) estimate of . Marks and Smith (2016) presented $_{\mathbf{N}}$ versus N for SARAL/AltiKa. Here, we present our results from Sentinel-3 A&B PLRM and SARM, along with those for SARAL/AltiKa (Figure 6).

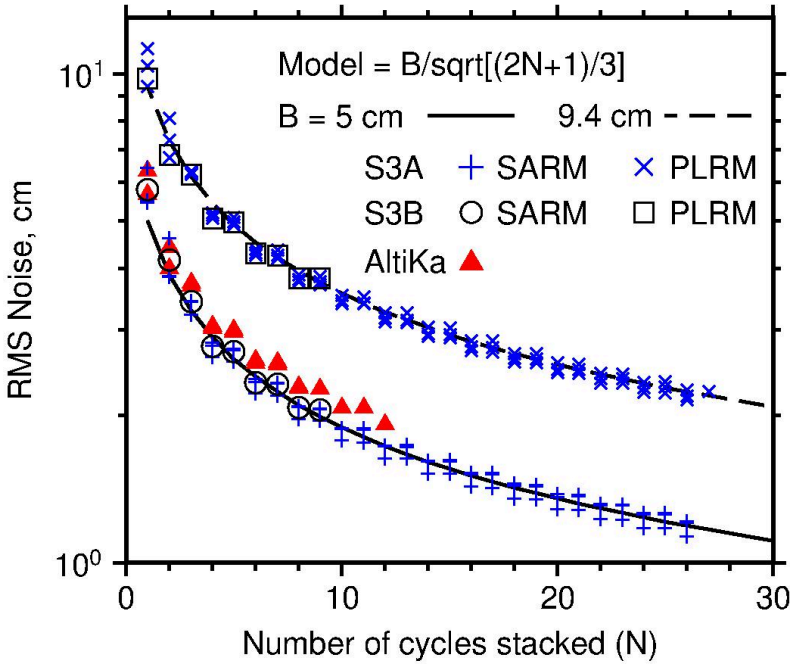

Figure 6. Root-mean-square (RMS) of sea surface height noise for Sentinel-3 A&B SARM and PLRM, and AltiKa, plotted against number of cycles stacked. Black curves are models for expected error in median stacks if the B value shown is the standard deviation in a single measurement.

The Sentinel-3 A&B SARM $_{\mathbf{N}}$ results give about 5 cm for $\mathbf{B} = _{\mathbf{1}}$ (the comparable value for SARAL/AltiKa is 5.6 cm (Marks and Smith, 2016)), and 1.2 cm

for a stack of 26 cycles. The Sentinel-3 A&B PLRM $_{\mathbf{N}}$ results give about 9.4 cm for $\mathbf{B} = _{\mathbf{1}}$ and 2.2 cm for a stack of 26 cycles. The B value for PLRM is about 1.9 times that for SARM, consistent with their comparative levels found above (Figures 1–4). B values from Sentinel-3 A appear the same as those from Sentinel-3B, which is expected, as the altimeters are identical.

6 Spectral Results

We compare the coherence and power spectra of Sentinel-3 A&B and SARAL AltiKa sea surface height profiles to estimate their resolution capabilities. We extracted data matrices after alignment and height adjustment that are sized 512 points by N columns (repeat cycle profiles) for Sentinel-3 A&B, and respectively 1024 by N for AltiKa; one alignment point is on featureless seafloor (Figure 7a) and two others are near the apices of seamounts (Figures 7b and 7c).

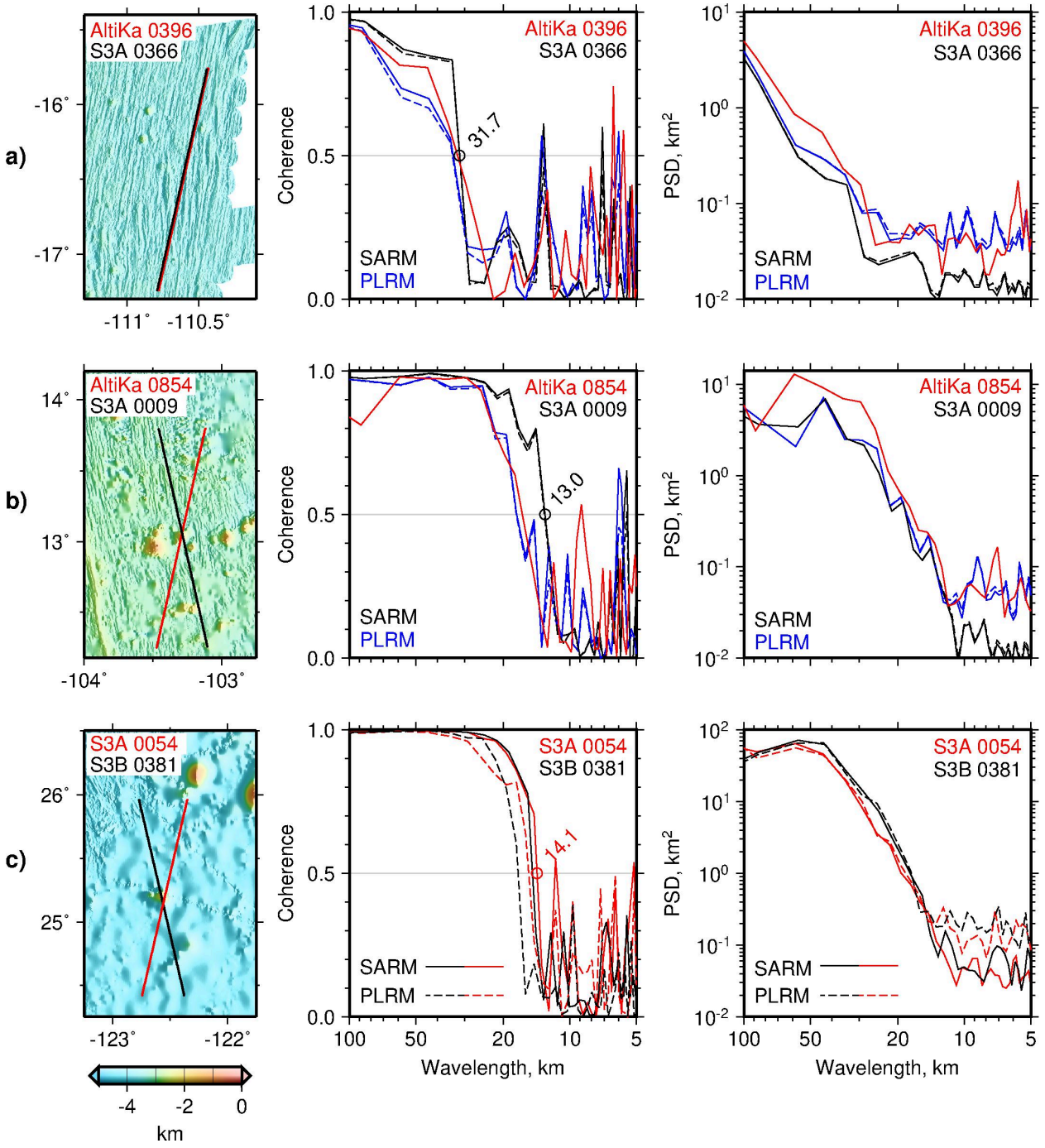

Figure 7. Panels show Coherence and Power Spectral Density (PSD) of selected passes over (a) area with no seamounts, (b) 1120 m tall seamount, and (c) 2130

m tall seamount. Solid and dashed lines in (a) and (b) are from stacks of 26 and 12 profiles, respectively (see text) and in (c), 19 profiles.

Power and coherence spectra were estimated from the average auto- and cross-spectra of the matrix profiles. Because two inputs are required for cross-spectral coherence analysis, two stacks were formed from each matrix described above. The number of profiles in a stack was the largest integer (M) that was less than or equal to half of the total number of repeat cycles available. Each stack was the median of 1024 random Monte Carlo realizations of M profiles. For Figures 7a and 7b, M=26 (solid lines) or 12 (dashed lines) for Sentinel-3, and M=12 for AltiKa; and for Figure 7c, M=19. Spectra from Sentinel-3 A&B and AltiKa stacks having the same number of profiles allows comparison of resolution between the altimeters, while spectra from stacks having the maximum number of available profiles demonstrates the highest resolution achievable. Coherence near 1 indicates nearly perfect correlation, while coherence near 0 indicates the absence of any significant linear relationship between the variance in one input with another input. A coherence of 0.5 may be considered as a signal-to-noise ratio of 1:1.

Figure 7a shows Sentinel-3A pass 0366 and adjacent AltiKa pass 0396. The spectral resolution of the two altimeters can be compared because of the proximity (and hence similar underlying topography) of the two passes, and because M was limited to 12 for Sentinel-3A (dashed lines) to match Altika (red line). The coherence plot demonstrates that Sentinel-3A (SARM and PLRM) and AltiKa are coherent to approximately 31.7 km wavelength. The PSD plot shows that the power is similar for Sentinel-3 and AltiKa at wavelengths longer than 31.7 km. The flattening of the curves at shorter wavelengths corresponds to the noise level: Sentinel-3A SARM has the lowest noise, with the level of Sentinel-3A PLRM and AltiKa being similar and higher than SARM. Sentinel-3 spectra from the maximum number of profiles in a stack ($M = 26$; solid lines) are nearly identical to spectra restricting M to 12 (dashed lines). This is because of upward continuation of seafloor signal to the sea surface.

Figure 7b shows Sentinel-3A pass 0009 and AltiKa pass 0854 that intersect over the apex of a 1120 m tall seamount. In this example Sentinel-3A SARM is coherent to 13 km wavelength, with Sentinel-3 A PLRM and AltiKa coherent to 17.5 km wavelength. Comparison of the coherence in Figure 7a over seafloor with no seamount, and Figure 7b over a small seamount, suggests that the 13 – 31.7 km waveband is associated with the seamount. The higher power spectral density in Figure 7b than in Figure 7a in the 13 - 31.7 km waveband likely reflects signal from the seamount. This waveband is in good agreement with the seamount waveband found by Marks and Smith (2016) in a spectral analysis of AltiKa data over areas with and without seamounts. The short-wavelength noise level in the power spectral density is lowest for Sentinel-3A SARM, and the Sentinel-3A PLRM and AltiKa noise levels are similar, and higher than for SARM.

Finally, we seek to compare the spectral characteristics of Sentinel-3A pass 0054

and B pass 0381, that intersect over a seamount 2130 m tall. Since 19 cycles were stacked for Sentinel-3B, we restricted 3A to 19 cycles as well. The coherence plot in Figure 7c shows that both Sentinel-3A and 3B SARM are coherent to about 14.1 km, with Sentinel-3 A&B PLRM coherent to slightly longer wavelengths (17.3 km). The power spectra density also shows corresponding power in the 13 - 31.7 km seamount waveband. The power spectral density noise level at short wavelengths shows that both Sentinel-3 A&B SARM have a lower noise level than Sentinel-3 A&B PLRM.

7 Summary

We described a method of stacking altimeter sea surface height data that we developed for SARAL/AltiKa but here customized and optimized for Sentinel-3. The method entails adjusting repeat cycle profiles for non-geoid height and height errors, aligning to common positions along a synthetic track, and calculating the median height profile. Four NetCDF files containing Sentinel-3 A&B SARM and PLRM median profiles at 1 km spacing are available for download from the NCEI data repository (Marks & Smith, 2020a, 2020b 2020c, 2020d).

Global maps produced from the stacking process demonstrate that nearly 88% of 512-point long chunks of Sentinel-3 repeat cycle data over oceans pass our selection criteria for inclusion in a stack, and that PLRM sigma values, the expected error in a single measurement, are about 1.9 times those of SARM. This is consistent with Sentinel-3 PRLM stacked height noise levels that are about 1.9 times those of SARM. SARAL AltiKa stacked height noise is close to that of Sentinel-3 SARM when the same number of cycles are stacked.

Our spectral analysis shows that small seamounts are similarly resolved by Sentinel-3 A&B and AltiKa median profiles. We compared power spectra and coherence from passes traversing seamounts and featureless seafloor. For passes over seamounts we interpret signal observed in the 13 – 31.7 km waveband as arising from the seamounts. This comports with the seamount waveband we determined from a similar AltiKa spectral analysis (Marks and Smith, 2016).

Because noise decreases with an increase in the number of cycles stacked, we expect median profiles from long-lived repeat cycle satellite missions to resolve shorter wavelengths and hence potentially smaller seamounts. Satellite tracks that lie between tracks of other satellites will enhance the identification of small seamounts on the global ocean seafloor and augment the seamount census.

Acknowledgments

We thank Eric Leuliette for Sentinel-3 repeat cycle data and helpful discussions. Unfiltered stacked sea surface height data are available for free download from the NCEI data repository (https://accession.nodc.noaa.gov/0219900, https://accession.nodc.noaa.gov/0219901, https://accession.nodc.noaa.gov/0219902, https://accession.nodc.noaa.gov/0219903. This work made use of MATLAB mathematical computing software from MathWorks (http://mathworks.com) and GMT software (Wessel & Smith, 1998; http://generic-mapping-tools.org).

The views, opinions, and findings contained in the report are those of the authors and should not be construed as an official National Oceanic and Atmospheric Administration or U.S. Government position, policy, or decision.

References

Donlon, C., Berruti, B., Buongiorno, A., Ferreira, M.-H., Féménias, P., Frerick, J., Goryl, P., Klein, U., Laur, H., Mavrocordatos, C., Nieke, J., Rebhan, H., Seitz, B., Stroede, J., & Sciarra, R. (2012), The Global Monitoring for Environment and Security (GMES) Sentinel-3 mission, *Remote Sensing of Environment, 120,* 37-57. doi:10.1016/j.rse.2011.07.024

Egido, A. & Smith, W. H. F. (2017), Fully focused SAR altimetry: theory and applications. *IEEE Transactions on Geoscience and Remote Sensing, 55*(1), 392–406. https://doi.org/10.1109/TGRS.2016.2607122

Kaula, W. M. (1966) *Theory of Satellite Geodesy*, Blaisdell.

Marks, K. M. & Smith, W. H. F. (2016), Detecting small seamounts in AltiKa repeat cycle data. *Marine Geophysical Research, 37*(4), 349-359. https://doi.org/10.1007/s11001-016-9293-0

Marks, K. M. & Smith, W. H. F. (2018), A method of stacking AltiKa repeat cycle data that may reveal 75,000+ possible small seamounts. *Earth and Space Science, 5*, 964-969. https://doi.org/10.1029/2018EA000440

Marks, K. M. & Smith, W. H. F. (2018), *Global Stacked Sea Surface Height Profiles from AltiKa Satellite Altimeter Data (NCEI Accession 0174134).* Version 1.1. Boulder, CO: NOAA National Centers for Environmental Information. Dataset. http://accession.nodc.noaa.gov/0174134. https://doi.org/10.25921/8hk9-fk45

Marks, K. M. & Smith, W. H. F. (2020a), *Global Stacked Sea Surface Height Profiles from Sentinel-3A Synthetic Aperture Radar Mode (SARM) Satellite Altimeter Data (NCEI Accession 0219900),* Version 1.1. Boulder, CO: NOAA National Centers for Environmental Information. Dataset. https://accession.nodc.noaa.gov/0219900. https://doi.org/10.25921/0rve-s239

Marks, K. M. & Smith, W. H. F. (2020b), *Global Stacked Sea Surface Height Profiles from Sentinel-3A Psuedo-Low Rate Mode (PLRM) Satellite Altimeter Data (NCEI Accession 0219901),* Version 1.1. Boulder, CO: NOAA National Centers for Environmental Information. Dataset. https://accession.nodc.noaa.gov/0219901. https://doi.org/10.25921/m0hw-a781

Marks, K. M. & Smith, W. H. F. (2020c), *Global Stacked Sea Surface Height Profiles from Sentinel-3B Syntheitc Aperutre Radar Mode (SARM) Satellite Altimeter Data (NCEI Accession 0219903),* Version 1.1. Boulder, CO: NOAA National Centers for Environmental Information. Dataset. https://accession.nodc.noaa.gov/0219903. https://doi.org/10.25921/wc1q-m472

Marks, K. M. & Smith, W. H. F. (2020d), *Global Stacked Sea Surface Height*

Profiles from Sentinel-3B Psuedo-Low Rate Mode (PLRM) Satellite Altimeter Data (NCEI Accession 0219902), Version 1.1. Boulder, CO: NOAA National Centeres for Environmental Information. Dataset. https://accession.nodc.noaa.gov/0219902. https://doi.org/10.25921/88xm-2k19

Pavlis, N. K., Holmes, S. A., Kenyon, S. C., & Factor, J. K. (2012), The development and evaluation of the earth gravitational model 2008 (EGM2008). *Journal of Geophsical Research, 117*, B04406. https://doi.org/10.1029/2011JB008916

Raney, R. K. (1998), The delay/Doppler radar altimeter. *IEEE Transactions on Geoscience and Remote Sensing, 36*(5), 1578–1588. https://doi.org/10.1109/36.718861

Sentinel-3 Team (2013), Sentinel-3 User Handbook (GMES-S3OP-EOPG-TN-13-0001). Paris, France: European Space Agency (ESA). http://sentinels.uat.esaportal.eu/documents/247904/685236/Sentinel-3_User_Handbook

Smith, W. H. F. (2015), Resolution of seamount geoid anomalies achieved by the SARAL/AltiKa and Envisat RA2 satellite altimeters. *Marine Geodesy, 38*(sup1). 644-671. https://doi.org/10.1080/01490419.2015.1014950

Telespazio VEGA Team, CLS, CNES (2017), Sentinel-3 Product Data Format Specification – SRAL/MWR Level 1 & 2 Instrument Products (S3IPF.PDS.003). Darmstadt, Germany:European Space Agency (ESA).

Wessel, P., & Smith, W. H. F. (1998), New, improved version of generic mapping tools released. *EOS, Transactions American Geophysical Union, 79*(47), 579. https://doi.org/10.1029/98EO00426